Alkali-activated materials for radionuclide immobilisation and the effect of precursor composition on Cs/Sr retention

Peer-reviewed author version

VANDEVENNE, Niels; Ion Iacobescu, Remus; CARLEER, Robert; SAMYN, Pieter; D'HAEN, Jan; Pontikes, Yiannis; SCHREURS, Sonja & SCHROEYERS, Wouter (2018) Alkali-activated materials for radionuclide immobilisation and the effect of precursor composition on Cs/Sr retention. In: JOURNAL OF NUCLEAR MATERIALS, 510, p. 575-584.

DOI: 10.1016/j.jnucmat.2018.08.045
Handle: http://hdl.handle.net/1942/26732

Alkali-activated materials for radionuclide immobilisation and the effect of precursor composition on Cs/Sr retention

Niels Vandevenne [a], Remus Ion Iacobescu [b], Robert Carleer [c], Pieter Samyn [c], Jan D'Haen[d,e], Yiannis Pontikes [b], Sonja Schreurs [a], Wouter Schroeyers [a,*]

[a] Hasselt University, CMK, Nuclear Technological Centre, Agoralaan, Gebouw H, 3590 Diepenbeek, Belgium

[b] KU Leuven, Department of Materials Engineering, Kasteelpark Arenberg 44, 3001 Leuven, Belgium

[c] Hasselt University, CMK, Research Group of Applied and Analytical Chemistry, Agoralaan, Gebouw D, 3590 Diepenbeek, Belgium

[d] Hasselt University, Institute for Materials Research (IMO), Wetenschapspark 1, 3590 Diepenbeek, Belgium

[e] IMEC, Division IMOMEC, Wetenschapspark 1, 3590 Diepenbeek, Belgium

* Corresponding author: Prof. Dr. Wouter Schroeyers, e-mail address: wouter.schroeyers@uhasselt.be

Abstract

One of the major challenges for the nuclear industry is the safe and sustainable immobilisation of radioactive wastes (RAW). Currently, the most commonly used immobilisation matrices for low and intermediate level wastes are based on ordinary Portland cement. For the more difficult to immobilise nuclides, such as caesium (Cs^+) and strontium (Sr^{2+}), researchers have been studying alternative immobilisation matrices, of which alkali-activated materials (AAM) are a very promising option. However, the differences in precursor compositions and the use of different types of activating solutions make it difficult to fully understand the effects of precursor composition on the immobilisation of introduced nuclides. Therefore, six different compositions of laboratory-synthesized Ca-Si-Al slags were developed to serve as precursors for low-alkaline AAMs to study their immobilisation behaviour. Immobilisation capacities up to 97.6 % Cs^+ and 99.9 % Sr^{2+} were achieved with 1 wt% waste loading when leaching for 7 days at 20 °C in Milli Q water. Cs^+ immobilisation is higher at lower Si/Al and Ca/(Si+Al) ratios. Immobilisation of Sr^{2+} is higher at a lower Ca/(Si+Al) ratio and independent of Si/Al ratio. The results of this study offer a deeper understanding of the immobilisation behaviour of AAMs and can encourage further research and application of AAMs for RAW immobilisation.

Keywords

Alkali-activated material; immobilisation; radioactive waste; caesium; strontium

1 Introduction

In the pursuit of a sustainable society, one of the main challenges for researchers and industries is the safe management and disposal of industrial wastes, with radioactive waste (RAW) being particularly important. RAW is produced by many different sources; the main ones being the energy sector (nuclear fuel cycle), the dismantling of nuclear installations, and applications in medicine, agriculture and industry. Because of the ever-increasing amounts of RAW, continuous innovation in immobilisation is becoming more and more important. As an alternative to the currently widely used cementitious immobilisation matrices, alkali-activated materials (AAM) have been increasingly studied. Depending on the type of precursor and the composition of the hydration products, AAMs (or subclasses thereof) are also known as geopolymers, inorganic polymers, soil cements, geocements, alkaline cements, zeoceramics, alkali-activated slag cement and a variety of other names [1,2]. AAMs have demonstrated promising results in immobilising radionuclides such as caesium and strontium [3-22]. As an example, the superior Cs^+ retention of AAMs was reported by *Shi and Fernández-Jiménez* (2006) [9], who tested leaching of Cs^+ and Sr^{2+} from AAMs containing zeolites and/or metakaolin (MK) as additives. They concluded that wastes show much less interference with the hydration of AAMs than that of ordinary Portland cement. *Blackford et al*. (2007) [11] developed a geopolymer matrix derived from MK, in which Cs^+ was introduced. They concluded that Cs^+ was fully incorporated into the amorphous geopolymer phase, proving the potential of AAMs for RAW immobilisation. In addition to the immobilisation of Cs^+ and Sr^{2+}, other elements such as Cd^{2+} and Pb^{2+} [23], and radionuclides such as ^{152}Eu, ^{60}Co, ^{59}Fe and isotopes of Am and Pu have also been successfully immobilised in AAMs [24–26].

Concerning the use of AAMs for RAW immobilisation, most literature covers AAMs based on commercial recipes, MK, fly ash (FA), ground granulated blast furnace slag (GGBFS) or combinations thereof. Despite the large body of research and the promising immobilisation results, a systematic study of the influence of the precursor composition on the immobilisation capacities for Cs^+ and Sr^{2+} is lacking. According to *Aly et al.* (2008) [12], MK-based AAMs show optimal leach resistance at Si/Al ratios higher than 2. They reported a sharp decrease in the Cs^+ release when the Si/Al ratio increased from 1.5 to 2 followed by a gradual increase at Si/Al ratios higher than 3, reaching the lowest value at Si/Al ratio of 2. For Sr^{2+}, the lowest release was obtained at a Si/Al ratio of 1.5, increasing gradually with increasing Si/Al ratio [12].

Almost all concerning literature describes AAMs made from industrial residues, making it difficult to exclude effects of trace elements in the precursor on the immobilisation capacities. Also, the variety in precursor origin and composition in most studies make it difficult to generalize the drawn conclusions, since the immobilisation performance is very dependent on the design parameters. In addition, there exists a wide variety of alkali-activators used, most often consisting of highly-alkaline activating solutions and often containing sodium silicates.

According to the IAEA [27], the lack of standards for precursors, experience of process optimization, and demonstration of long-term stability limit their use in RAW immobilisation, despite the reported favourable experiences using AAMs. They stated that novel materials need a better benchmarking, and emphasised that it is also important to realise that existing test methods do not always give comparable results with different classes of materials [27]. Therefore, the effect of precursor composition on the immobilisation of Cs^+ and Sr^{2+} in AAMs is studied in this work, by developing synthetic Ca-Si-Al slag precursors with different compositions from laboratory reagents, yielding Si/Al and Ca/(Si+Al) molar ratios of 0.95 – 5.1 and 0.42 – 1.0 respectively. In this way, immobilisation is studied excluding possible effects of trace elements in the mixture. The present results can be further used as a guideline for choosing industrial residues with a proper composition or for using proper mixing ratios.

2 Materials and methods

2.1 Ca-Si-Al slag synthesis

Ca-Si-Al slags were synthesised from analytical grade laboratory reagents Al_2O_3, SiO_2 and $CaCO_3$ (all Sigma-Aldrich, > 99 % pure). The studied compositions (**Table 1**) were chosen to broadly resemble GGBFS and to be fully liquid at 1550 °C (see **Figure 1**). The $CaCO_3$ was first calcined in a muffle furnace at 1050 °C overnight to expel CO_2. For each composition, the exact mass of $CaCO_3$ necessary for achieving the stoichiometric amount of CaO was weighed and inserted into the muffle furnace.

Immediately after cooling, the mass of the obtained CaO was determined to verify the complete decarbonation. The resulting CaO was then mixed with weighed amounts of Al_2O_3 and SiO_2 for two hours in a Turbula T2C mixer for homogenization. The mixtures were placed in a platinum crucible and inserted into a bottom loading furnace (AGNI ELT 160-02) at 1630 °C. A higher temperature was applied to account for possible differences in temperature between the location of the crucible and the thermocouple of the furnace, to ensure that the sample would melt completely. After an isothermal period of 2.5 h, the melt was quenched by pouring in water at room temperature. The cooled slag was then dried at 110 °C to constant weight before being crushed and milled in a Retsch disk mill RS200 at 1000 rpm for 60 s.

Homogeneity of the finely milled slag was confirmed by X-ray diffraction spectroscopy (XRD). The measurements were performed with a Bruker D8 diffractometer. This theta-theta diffractometer is equipped with a Göbel mirror (line focus, Cu k_α radiation). The X-rays are detected with a 1D lynxeye detector.

The specific surface area of the resulting powders was measured in threefold by use of Blaine method. The procedures described in the standard EN 196-6 [28] were followed as closely as possible and the measurements were performed against a reference cement sample. It is, however, important to note that the Blaine method is designed for cements and that results may deviate when using other types of materials.

Table 1: Designed compositions of synthetic slags (wt fraction) and the initial Si/Al and Ca/(Si+Al) molar ratios. The labelling of the samples is based on the initial Si/Al ratio.

	SiO_2 *wt* fraction	Al_2O_3 *wt* fraction	CaO *wt* fraction	Si/Al *mol/mol*	Ca/(Si+Al) *mol/mol*
S_1	0.37	0.33	0.30	0.95	0.42
S_1.1	0.40	0.30	0.30	1.1	0.43
S_2	0.49	0.21	0.30	2.0	0.44
S_2.4	0.47	0.17	0.36	2.4	0.59

S_3.4	0.40	0.10	0.50	3.4	1.0
S_3.4b*	0.40	0.10	0.50	3.4	1.0
S_5.1	0.60	0.10	0.30	5.1	0.45

**This composition, randomly chosen, has been made as a replicate to check the reproducibility of the experimental design*

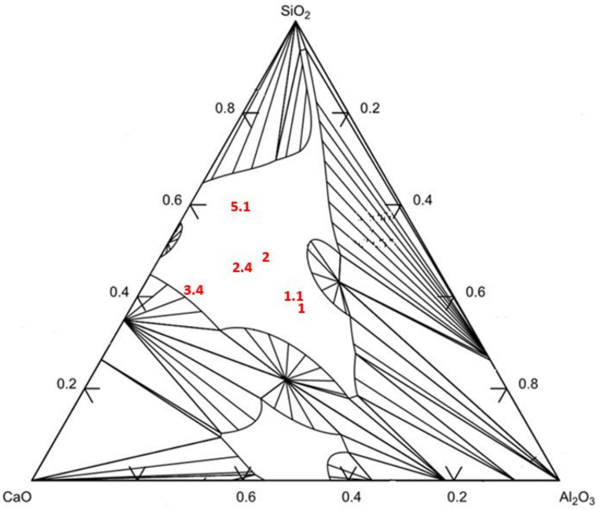

Figure 1: Phase diagram at 1550 °C. The designed compositions are all within the liquid (white) area.

2.2 AAM elaboration

AAM pastes were prepared by mixing the powdered slag precursors with a 2 M NaOH solution (prepared from NaOH pellets (Fischer Scientific, 98.44 % pure) and type II distilled water) using a laboratory mixer and maintaining a liquid to solid ratio (L/S) of 0.30. These parameters were chosen based on our earlier study [29] and adjusted for optimal workability and setting time. At this molarity and L/S ratio, the amount of Na^+ added is 1 wt% for each sample. Cs^+ and Sr^{2+} were added as nitrates ($CsNO_3$, Alfa Aesar 99.8%; $Sr(NO_3)_2$, Emsure 99.0%) to account for 1 wt% and 0.1 wt% respectively of the final AAM-mass (solid precursor + activating solution). A lower wt% of Sr^{2+} was chosen to avoid significant interference with the polymerisation kinetics, as reported in our earlier studies [29,30]. The resulting mixtures were poured into plastic (polymethylmethacrylate, PMMA) 25 x 25 x 20 mm^3 moulds. The moulds were manually tapped during 60 seconds to remove air bubbles before being sealed with a PMMA cap. These pastes were then allowed to cure for 28 days at 23 ± 1 °C. Each composition was made in threefold for the leaching experiments.

2.3 Leaching of introduced and structural elements

The release of introduced caesium and strontium, and of the structural elements silicon, aluminium, calcium and sodium was measured using a semi-dynamic diffusion test described in our earlier study [29] and based on the standards ASTM C1220-98 [31] and CEN/TS 15863:2015 [32]. The samples were demoulded, cleaned with a dry brush and measured for dimensions and weight before being submerged in 400 ml of pre-heated Milli-Q water (90 °C, polypropylene bottle and sample holder). Before and after the eluate was refreshed, the mass of the closed container was measured to determine water loss through evaporation. In all cases, the loss of mass through evaporation was lower than 2 %, which is in line with the standard ASTM C1220-98 [31]. At each sampling time (1 h, 24 h, 7 d, 28 d), 10.0 ml of the eluate was filtered over a 0.2 µm syringe filter and acidified immediately after sampling to a concentration of 2 % HNO_3 (MERCK Suprapur 65 %). The concentrations of water-soluble Sr^{2+}, Si^{4+}, Al^{3+}, Ca^{2+}, and Na^+ were measured by ICP-OES (Perkin Elmer type Optima 8300) in axial mode. The concentration of water-soluble Cs^+ was measured by ICP-MS (Perkin Elmer NexION 350S). At each sampling time, the eluate was also measured for pH (calibrated electrode HI1043B, Hanna Instruments) and conductivity (Schott Geräte CG 858, calibrated with 0.1 M KCl).

The release r (mg/m²) of element i at leaching interval n is calculated as:

$$r_{i,n} = \frac{\left(C_{i,n} - B_{i,n}\right) \cdot V}{A_s} \tag{1}$$

With

$C_{i,n}$ = concentration of element i in the filtered aliquot of leaching interval n (mg/ml)

$B_{i,n}$ = concentration of element i in the filtered blanc aliquot of leaching interval n (mg/ml)

V = initial volume of eluate in the bottle containing the sample AAM (ml)

A_s = geometric surface area of the sample AAM (m²)

The cumulative release R (mg/m^2) of each constituent is calculated as:

$$R_i = \sum_0^n r_{i,n} \tag{2}$$

The normalized leach rate LR (mg/(m^2.s)) of element i at leaching interval n is calculated as:

$$LR_{i,n} = \frac{r_{i,n}}{\Delta t_n \cdot f_i} \tag{3}$$

with Δt_n the time of leaching interval n (in seconds) and f_i the fraction of element i in the sample, as to account for possible differences in waste loadings. The total release of element i ($\%\,release_i$) and the percentage of wash-off in the first leaching interval ($\%WO_i$) are defined as:

$$\%\,release_i = \frac{R_{i,28d} \cdot A_s}{m_s \cdot f_i} \cdot 100\ \% \tag{4}$$

$$\%WO_i = \frac{R_{i,1h}}{R_{i,28d}} \cdot 100\ \% \tag{5}$$

with m_s the mass of the sample (mg) after demoulding.

2.4 *Effect of leaching temperature and specific surface area on immobilisation performance*

To confirm the observed relation between immobilisation capacity and the AAM design ratios, the immobilisation capacity of selected compositions has been tested under varying conditions. Samples of compositions AAM_1, AAM_1.1, AAM_2 and AAM_5.1 were leached at a lower temperature of 20 ± 1 °C for 7 days. The specific surface area of these samples was measured. The Brunauer Emmett Teller (BET) surface area, was measured for these samples by continuous flow method using 0.3 ml/min of nitrogen gas (Tristar 3000).

2.5 *Effect of slag fineness on immobilisation performance*

The effect of slag fineness on the immobilisation performance is studied by further milling slag precursors S_1 and S_2 for an additional 30 s. From these finer slags, additional samples of composition AAM_1 and AAM_2 were prepared for leaching during 7 d at 20 ± 1 °C.

3 Results and discussion

3.1 *Homogeneity of the slag*

All mixtures were completely molten during the isothermal period in the bottom loading furnace. Water-quenching of the melt gave rise to a clear transparent glass for all mixtures. XRD patterns of selected slag samples S_1.1, S_2.4, S_3.4 and S_5.1 are presented in **Figure 2**. No crystalline phases were detected in any of the measured slags, indicating homogeneity without crystalline inclusions.

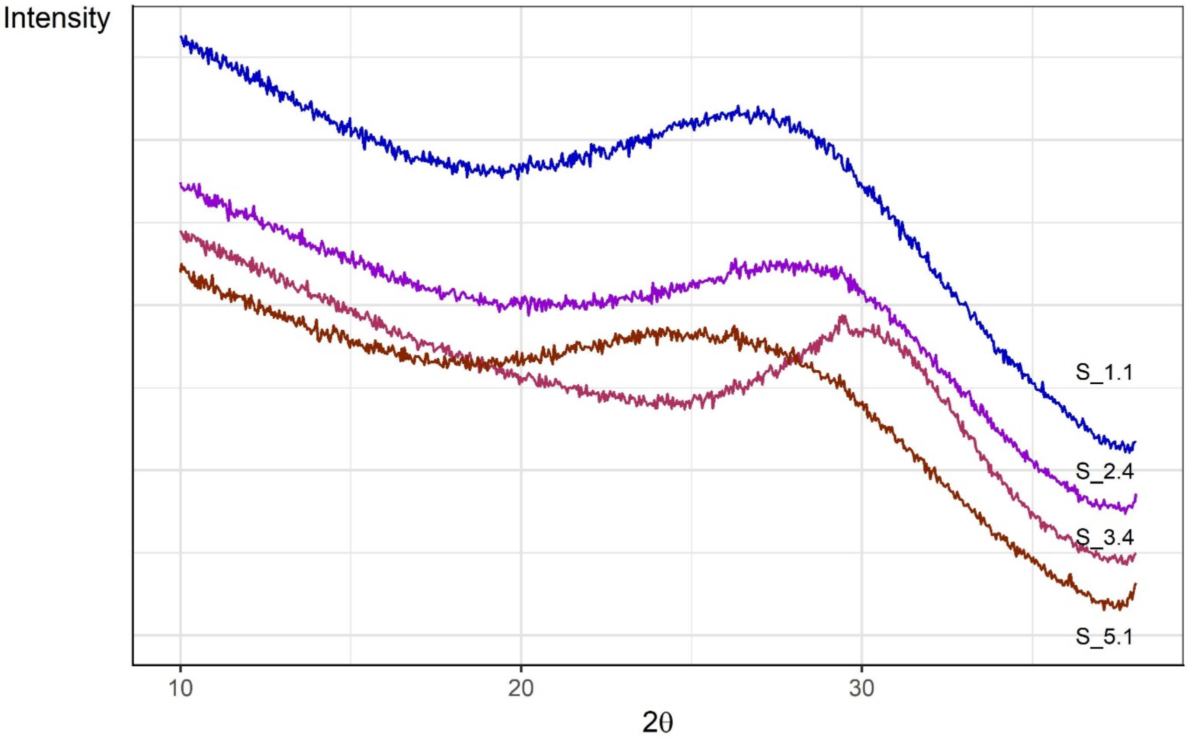

Figure 2: XRD patterns of the finely milled slags S_1.1, S_2.4, S_3.4 and S_5.1.

3.2 Immobilisation of Cs^+, Sr^{2+} and Na^+

Figure 3 shows the cumulative release for Cs^+, Sr^{2+} and Na^+ in function of the leaching time. The $\% \, release$ is summarized in **Table 2**. The highest Na^+ leaching is measured in AAM_5.1, which is also the sample with the highest Si/Al ratio. AAM_1.1 shows the best Cs^+ immobilisation, releasing only 7.8 ± 0.3 % of the introduced Cs^+, which is almost twice as good as the second best (AAM_1). In our earlier study [29], GGBFS-based AAMs activated with 6 M NaOH were leached for 7 days under the same conditions. The composition of the GGBFS closely resembles that of S_3.4 (excluding the contribution of MgO, SO_3 and other trace elements). With a 1 wt% Cs^+ loading, the GGBFS-AAM leached 66 % of the introduced Cs^+ [29]. This is much higher than the Cs^+ release observed in AAM_3.4 and AAM_3.4b which could be due to e.g. the differences in activating solution molarity or the presence of magnesium and other elements. Among the compositions tested in this study, AAM_3.4 performs worst regarding both Cs^+ and Sr^{2+} immobilisation indicating that the composition of GGBFS requires optimisation regarding immobilisation purposes.

The Cs^+ and Sr^{2+} normalized leach rates are given in **Table 3**. The effect of initial wash-off ($\%WO_{Cs}$) seems to be the least pronounced for AAM_1.1 (see **Table 3**) with a percentage released in the first hour of leaching of 7 % of the total amount leached. Also for Sr^{2+}, AAM_1.1 clearly shows the best immobilisation, releasing only 0.50 ± 0.04 % of the introduced Sr^{2+}, which is about 50 % better than the second best (AAM_2). The overall percentage of wash-off ($\%WO_{Sr}$, see **Table 3**) is lower for Sr^{2+} than for Cs^+ indicating a slower release from the sample surface.

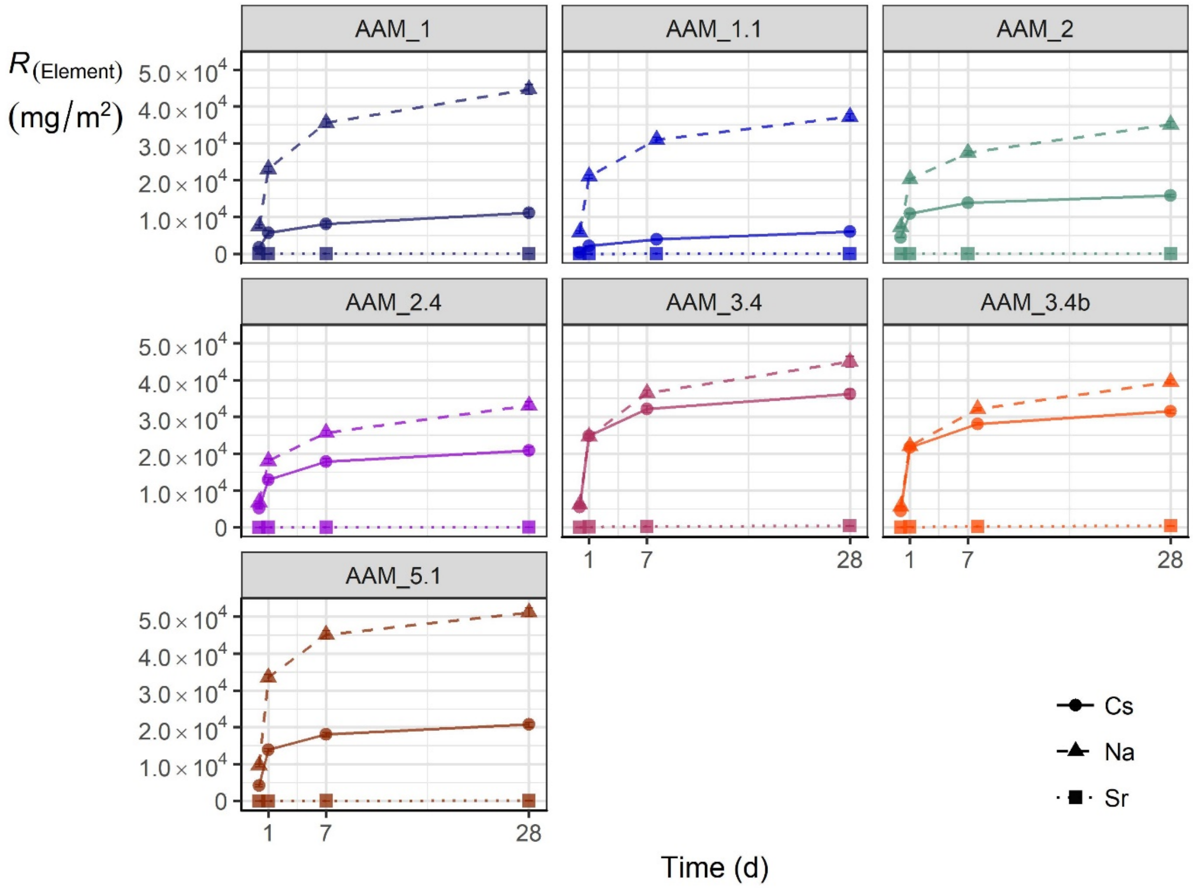

Figure 3: Cumulative release of Cs^+, Na^+ and Sr^{2+} during a 28-d leaching test at 90 °C.

Table 2: Percentage of introduced Cs^+, Sr^{2+} and Na^+ that has been released by leaching for 28 d at 90 °C. Uncertainties are calculated as standard deviations from 3 samples per composition.

$\% \, release_i$	Cs^+	Sr^{2+}	Na^+
AAM_1	14 ± 2	1.11 ± 0.07	58 ± 2
AAM_1.1	7.8 ± 0.3	0.5 ± 0.04	49 ± 2
AAM_2	20.1 ± 0.5	0.74 ± 0.3	46 ± 1
AAM_2.4	40 ± 2	1.4 ± 0.2	65 ± 2
AAM_3.4	46 ± 2	4.9 ± 0.5	59 ± 2
AAM_3.4b	40.9 ± 0.7	5 ± 0.4	53 ± 1
AAM_5.1	27.8 ± 0.9	0.9 ± 0.1	71 ± 2

Table 3: Average leach rates (mg/(m².s)) of Cs^+ and Sr^{2+} during a 28-d leaching period at 90 °C. The mean value calculated per sample is weighted for the time of the respective leaching interval. $\%WO_i$ (wash-off) is the percentage of the total released amount leached in the first hour of the test.

	Leaching time (h)	AAM_1	AAM_1.1*	AAM_2	AAM_2.4	AAM_3.4	AAM_3.4b*	AAM_5.1
$\boldsymbol{LR_{Cs}}$	1	49	12	120	150	150	120	120
	24	4.7	2.0	7.8	9.3	23	21	12
	168/ 192*	0.47	0.30	0.55	0.94	1.4	1.1	0.80
	672	0.13	0.09	0.09	0.13	0.18	0.14	0.12
Mean		0.43	0.23	0.64	0.83	1.5	1.3	0.83
$\%\boldsymbol{WO_{C}}$		*16*	*7*	*28*	*25*	*15*	*14*	*20*
$\boldsymbol{LR_{Sr}}$	1	0.68	0.53	0.39	1.5	10	12	0.77
	24	0.14	0.070	0.24	0.36	0.94	1.1	0.20
	168/ 192*	0.047	0.017	0.036	0.035	0.27	0.22	0.033
	672	0.022	0.0089	0.0079	0.0088	0.054	0.049	0.012
Mean		0.032	0.014	0.023	0.029	0.15	0.15	0.024
$\%\boldsymbol{WO_{S}}$		*3*	*5*	*2*	*8*	*10*	*11*	*4*

The overall leaching behaviour as seen in **Figure 3** is comparable for all samples and comprises a decreasing leaching rate with increasing leaching time. E.g. LR_{Cs} for AAM_1 is 49 mg/(m².s) in the first hour of leaching, decreases with a factor 10 for each following step (24 h, 7 d) and levels off in the final interval (see **Table 3**). For both Cs^+ and Sr^{2+}, the leach rate for all samples is highest in the first hour of leaching. This behaviour is typical for materials with an initial surface wash-off, which is a process that occurs often in this type of tank test for monolithic materials and comprises the fast dissolution of soluble salts from the surface of the monolith [33]. In addition to surface wash-off, diffusion of the element of interest through the sample and eventual depletion of the element from the sample are important processes governing the leaching behaviour.

Diffusion-controlled release from a monolithic waste form is related to the surface area of the waste form and the time of exposure [33]. In semi-dynamic tank leaching tests with a monolithic sample, a one-dimensional semi-infinite diffusion model, based on Fick's second law, is often assumed [34,35].

In this model, mass transfer is assumed to take place in response to concentration gradients in the pore water solution of the structure [35]. When Fickian diffusion is considered as the dominant release mechanism, the mass release should be proportional to the square root of the release time ($R \sim t^{0.5}$); this results in a straight line with a slope of 0.5 when the logarithm of the cumulative release is plotted against the logarithm of the release time [35]. Initial surface wash-off causes a higher release in the first stage of leaching, while depletion leads to a levelling-off of the cumulative release curve [33].

Figure 4 shows the cumulative **caesium and strontium** release of a selected subset of samples (the remaining samples show similar behaviour) plotted against the release time on a double logarithmic scale. None of the samples closely follow the 0.5 slope. Since an initial wash-off and depletion of Cs^+ is clear from **Table 2** and **Table 3**, the results from the leaching test can be divided into the intervals [1 h ; 24 h] and [24 h ; 28 d] as shown in **Figure 4a** for Cs^+ and **Figure 4b** for Sr^{2+}.

For **caesium**, it is clear from **Figure 4a** that the sample with limited wash-off (AAM_1.1, as seen in **Table 3**) has a slope close to 0.5 in the interval [1 h ; 24 h] indicating possible diffusion-controlled release. AAM_2 shows a slope of 0.28 in this first interval, indicating a significant wash-off (high concentration in the first hour of leaching).

In the interval [24 h ; 28 d], the regression lines flatten for all samples (slope < 0.5) indicating signs of depletion. Since depletion is only assumed to occur when the total release is higher than 20 % [35], not all samples have actually been significantly depleted. **Table 2** shows that the release of Cs^+ from the AAMs is between 46 and 7 %. The fact that depletion-like behaviour occurs even in samples with a low release indicates a possible distribution of the present Cs^+ into an easily-leachable fraction and a strongly-bound fraction. The occurrence of the wash-off and the depletion effects can then be contributed to the easily-leachable fraction. The levelling-off of the regression curve could thus be caused by the depletion of the readily available Cs^+, while the remaining fraction is more strongly bound in the AAM structure. The leaching behaviour of Cs^+ can thus be summarized as a combination of initial wash-off, diffusion, and depletion of an easily-released fraction. The lower the Si/Al and Ca/(Si+Al) ratio, the smaller this easily-leachable fraction (as discussed further).

For **strontium**, the leaching behaviour in most samples does not seem to be dependent on the leaching interval as seen in **Figure 4b**. The overall slopes of the regression curves are smaller than 0.5, indicating depletion. Since the total amount of leached Sr^{2+} is small for all samples (< 5 %, see **Table 2**), it seems reasonable that Sr^{2+} leaches only from the sample surface, slowly depleting while the bulk of the Sr^{2+} remains encapsulated in the sample, not available for leaching.

The amount of **sodium** leached does not correspond with the amount of Cs^+ leached (see **Table 2**), as would be expected since Cs^+ is known to act as a charge-balancing ion, replacing Na^+ in the framework [13,15]. This indicates that Cs^+ and Na^+ immobilisation is not completely similar, and shows that Cs^+ is retained better than Na^+ (since Na^+ release is higher and both were introduced as 1 wt%). This is consistent with the findings of *Kuenzel et al.* (2015) [15], who reported that the reaction between Cs^+ and $Al(OH)_4^-$ is favoured over that of Na^+ because of the lower charge density of Cs^+. In addition, the difference in immobilisation between Cs^+ and Na^+ is dependent on the AAM composition, since from **Table 2** it can be seen that e.g. AAM_2 releases the least Na^+ (46 %) while releasing 20 % Cs^+; in contrast, AAM_1 leaches less Cs^+ (14 %) and more Na^+ (58 %). This could indicate a difference in hydrate phases formed depending on the AAM composition. The findings of *Kuenzel et al.* (2015) [15] were based on MK-AAMs, resulting in an amorphous sodium aluminosilicate hydrate (N-A-S-H) as the main binder phase.

A difference in the amount of N-A-S-H formed (as compared to calcium sodium aluminosilicate hydrate (C-(N)-A-S-H)) could be the cause of the difference in leaching behaviour of Na^+ as compared to Cs^+. Based on the initial composition of the slags and the use of a NaOH activator, the AAMs are expected to consist mainly of C-(N-)A-S-H gel, N-A-S-H gel (due to high Al content), strätlingite, and some zeolitic phases [36–38]. For the low Si/Al samples AAM_1 and AAM_1.1, the ratio of leached Na^+/Cs^+ is much higher than for the high Si/Al samples (see **Table 2**).

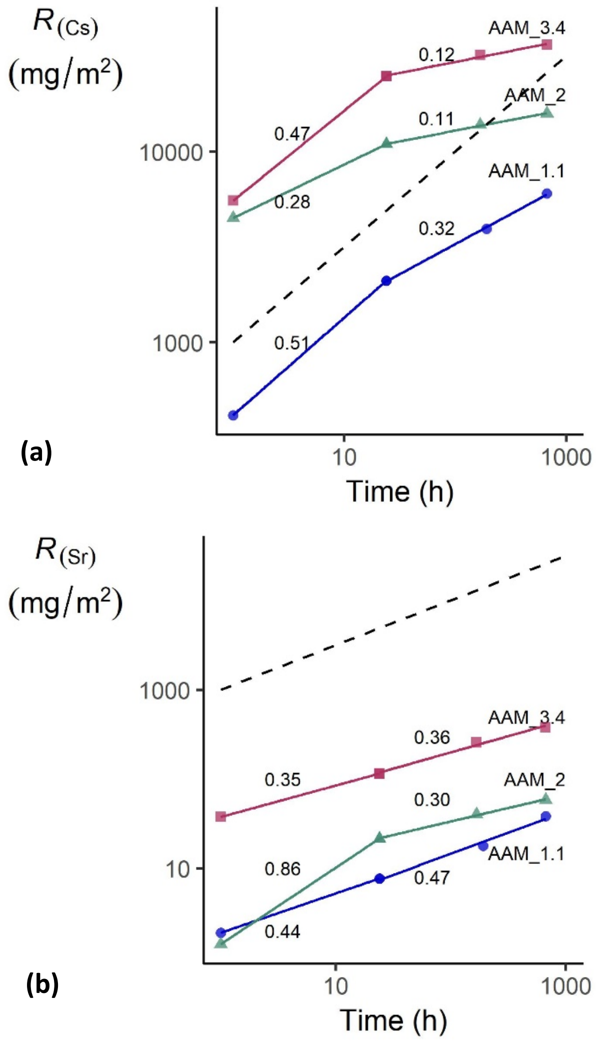

Figure 4: (a) R_{Cs}, dividing the leaching time into two intervals [1 h ; 24 h] and [24 h ; 28 d] and **(b)** R_{Sr}, dividing the leaching time into two intervals. R^2-values are all > 0.97 for **(a)** and **(b)**. The dashed line represents the slope of 0.5 from a diffusion-based release. The slopes are indicated on the graph next to the regression lines.

When linking the immobilisation capacity for Cs^+ and Sr^{2+} with the precursor composition, an initial Si/Al ratio of about 1.1 (**Table 2**) seems to be best. **Figure 5a** shows the cumulative 28-d release of Cs^+ in function of the Si/Al and Ca/(Si+Al) ratios of the precursor slags. For the studied compositions, Cs^+ is immobilised better in AAMs with lower Si/Al ratios and lower Ca/(Si+Al) ratios.

Figure 5b shows the cumulative 28-d release of Sr^{2+} in function of the Si/Al and Ca/(Si+Al) ratios of the precursor slags. For the studied compositions, the immobilisation of Sr^{2+} is dependent on the Ca/(Si+Al) ratio, but not on the Si/Al ratio. This indicates a competition between Ca^{2+} and Sr^{2+} for incorporation into the AAM structure. The independence of strontium leaching to the Si/Al ratio is in contrast with the results of the study of *Aly, et al.* (2008) [12], where Sr^{2+} release increased in samples with an increasing Si/Al ratio from 1.5 to 4. This could be due to the fact that the samples studied by *Aly, et al.* (2008) [12] were low in calcium, indicating the possible differences in leaching behaviour in function of the type of AAMs.

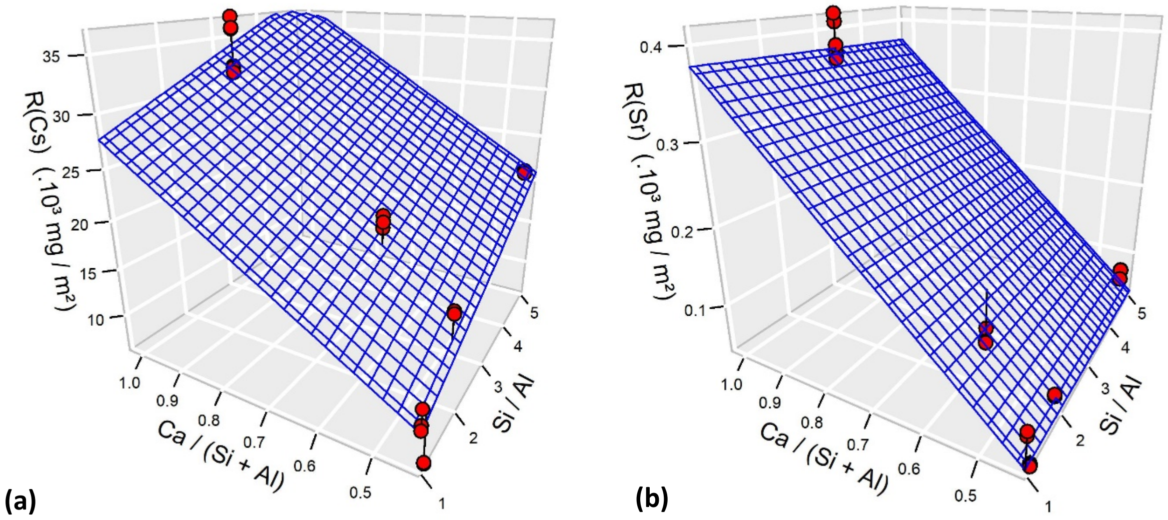

Figure 5: The cumulative 28-d release of Cs^{+} **(a)** and Sr^{2+} **(b)** (10^3 mg/m²) in function of the Si/Al and Ca/(Si+Al) ratios of the precursor slags. The regression planes are a result of multiple linear regressions with R^2-values > 0.93.

3.3 Release of structural elements

The Ca^{2+} release of AAM_1, AAM_1.1, AAM_3.4 and AAM_3.4b are similar, while S_1 and S_1.1 have a CaO content of only 30 % and S_3.4 and S_3.4b have an initial CaO content of 50 %. Also, the Ca^{2+} release decreases with increasing Si/Al ratio reaching a value of 7300 ± 200 mg/m² for AAM_2 and 5000 ± 200 mg/m² for AAM_5.1. This higher Ca^{2+} release at lower Si/Al ratios explains why AAM_1, AAM_1.1, AAM_3.4 and AAM_3.4b show a similar Ca^{2+} release while having a lower calcium content.

This behaviour of calcium leaching could be an indication of less C-(N)-A-S-H formation at lower Si/Al ratios since the formation of this phase would better immobilise Ca^{2+} into the structure. An increased Al content (and thus lower Si/Al ratio) promotes the formation of N-A-S-H in addition to C-(N)-A-S-H, while an increased Ca content impedes the formation of N-A-S-H [38]. Higher Si/Al ratios will thus give rise to more C-(N)-A-S-H formation.

The highest **silicon** release is observed in AAM_5.1 (≈ 24 000 mg/m²), while AAM_3.4, AAM_3.4b, and AAM_1.1 show the lowest silicon release (≈ 5000 mg/m²). AAM_2.4, AAM_2, and AAM_1 all show a 28-d cumulative silicon release around 10 000 mg/m². The lower silicon leaching of AAM_3.4 and AAM_3.4b as compared to AAM_2.4, AAM_2, and AAM_1 (while having similar initial SiO_2 contents) indicates that a higher calcium content increases the immobilisation of silicon, which again indicates the formation of C-(N)-A-S-H.

Regarding **aluminium**, the release follows the Si/Al ratio, with AAM_5.1 showing the lowest aluminium release and increasing with decreasing Si/Al. For AAM_1, the amount of silicon and aluminium released is almost equal (AAM_1: R_{Si} = 10000 ± 600 mg/m², R_{Al} = 9200 ± 500 mg/m²), indicating congruent dissolution.

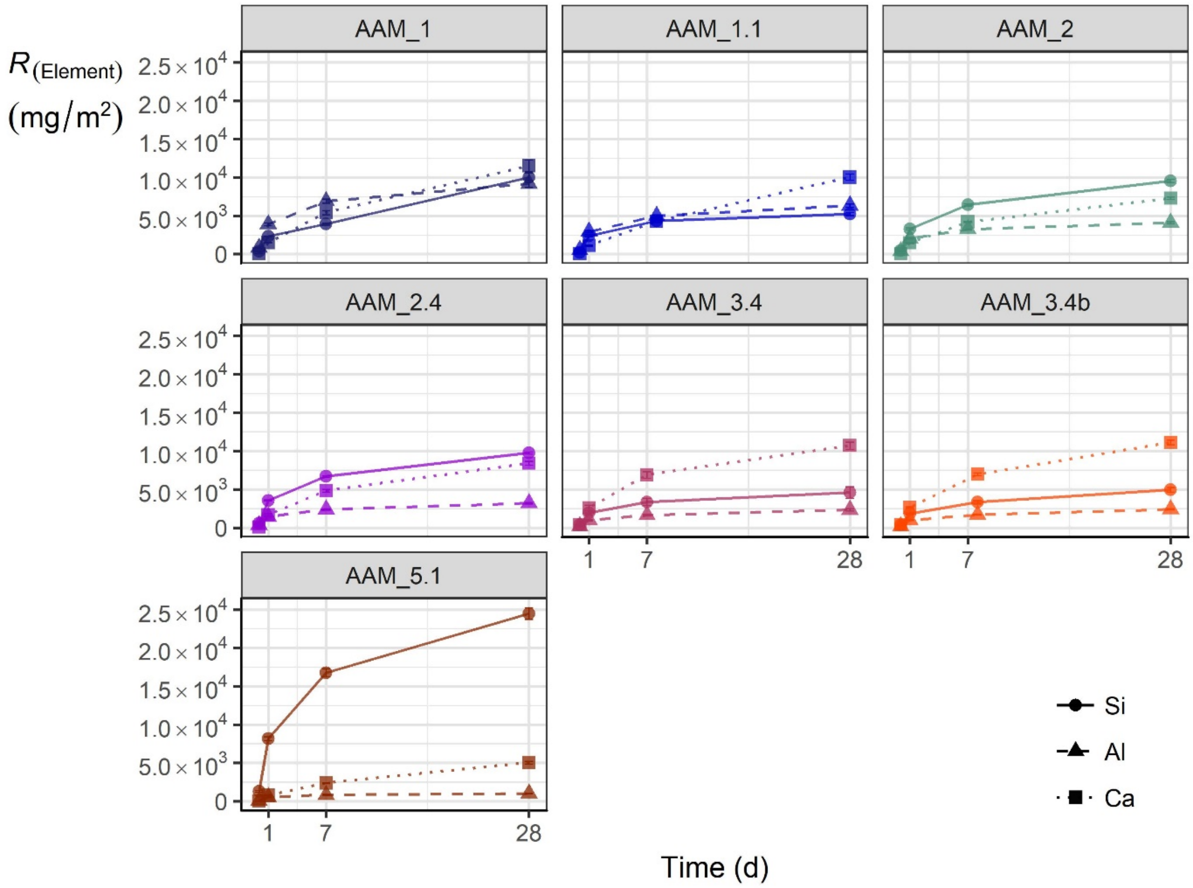

Figure 6: Cumulative release of silicon, aluminium and calcium during a 28-d leaching test at 90 °C.

3.4 pH and conductivity

The measured pH of the eluates was similar for all samples. After 1 h of leaching the average pH over all samples was 10.7 ± 0.3. After 24 h, the pH of the eluates increased to 11.2 ± 0.3. After 28 d, the pH-values were 11.3 ± 0.6. The conductivity of selected eluates is given in **Figure 7**.

AAM_5.1, AAM_3.4, AAM_3.4b, AAM_2.4 and AAM_2 show a high peak in conductivity at 24 h (only AAM_2 and AAM_3.4 shown in **Figure 7**), while decreasing at later sampling times. This high early peak in ionic conductivity followed by a gradual decrease indicates a more profound early wash-off and subsequent depletion, which is consistent with the results seen for Cs^+ in **Figure 4a**. This effect is not so pronounced for AAM_1.1, which shows a slighter decrease in conductivity at the 7 d sampling time. Regarding the validity of the experimental design, the duplicates AAM_3.4 and AAM_3.4b show very similar results in all measured leaching aspects, confirming that the slag development, the AAM development, and the leaching tests are very well reproducible.

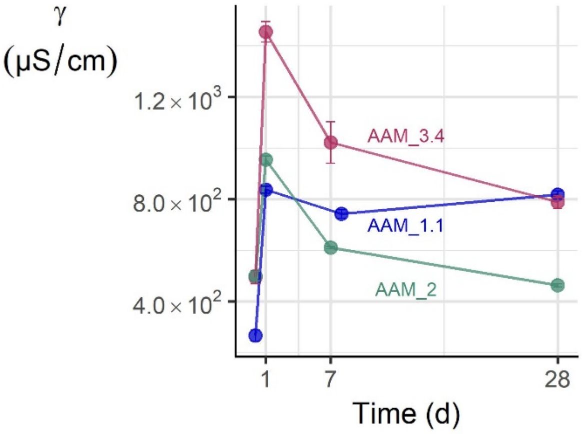

Figure 7: Conductivity values (µS/cm) of AAM_1.1, AAM_2 and AAM_3.4 at each sampling time.

3.5 Effect of leaching temperature on immobilisation capacity

Table 4 and **Table 5** show that the leaching temperature has a profound effect on the release of all constituents. However, this effect is not the same for all samples. AAM_1 exhibits significantly less release at 20 °C than at 90 °C for Cs^+, Sr^{2+} and Na^+, while AAM_5.1 exhibits less release for Sr^{2+} and Na^+ but not for Cs^+. In contrast, AAM_1.1 has a significantly higher release at 20 °C as compared to 90 °C for all constituents, while AAM_2 has a higher release for Cs^+ and Na^+ at 20 °C and a similar release for Sr^{2+}. Although all samples were completely set after 28 days of curing, it appears that the high temperature (90 °C) of the leaching environment influenced the curing of AAM_1.1 and AAM_2 which significantly improved their immobilisation potential. This does not seem to be the case for AAM_1 and AAM_5.1.

Table 4: Slag Blaine values, $\%\,release$ and BET values for samples leached for 7 d at 20 °C. The $\%\,release$ values are given as individual measurements since only one or two samples were tested per composition.

	Slag Blaine (m²/kg)	$\%\,release$ 7 d, **20 °C**			BET (m²/g)
Sample		Cs$^+$	Sr^{2+}	Na$^+$	
AAM_1	110 ± 20	2.97; 3.06	0.13; 0.22	31.52; 31.77	10.7 ± 0.1
AAM_1.1	200 ± 20	11.22	4.02	60.21	14.8 ± 0.1
AAM_2	140 ± 10	26.56; 27.94	0.27; 0.49	41.29; 42.76	3.8 ± 0.1
AAM_5.1	310 ± 10	22.45; 22.71	0.20; 0.22	53.88; 55.21	37.5 ± 0.1

Table 5: Percentages of Cs$^+$, Sr^{2+} and Na$^+$ released after 7 d leaching at 90 °C.

	$\%\,release$ 7 d, **90 °C**		
Sample	Cs$^+$	Sr^{2+}	Na$^+$
AAM_1	10 ± 1	0.48 ± 0.05	46 ± 2
AAM_1.1	5.1 ± 0.2	0.23 ± 0.03	41 ± 1
AAM_2	17.5 ± 0.3	0.51 ± 0.2	36 ± 1
AAM_5.1	24.2 ± 0.7	0.49 ± 0.06	62 ± 2

3.6 Effect of specific surface area on immobilisation capacity

The BET specific surface area (before leaching) of the samples used for leaching at 20 °C is given in **Table 4**. The BET specific surface area is lowest for AAM_2, while AAM_5.1 exhibits the highest BET area. The specific surface areas of AAM_1 and AAM_1.1 are comparable. AAM_2 releases more Cs$^+$ and Sr^{2+} than AAM_5.1 at 20 °C, although having a much lower BET value. From the tested samples, no clear correlation could be established between the BET values and the immobilisation capacities.

3.7 Effect of slag fineness on immobilisation capacity

The remainder of slag precursors S_1 and S_2 were further milled for an additional 30 s. The higher Blaine values (HB) of these slags are given in **Table 6**. From these finer slags, additional samples of composition AAM_1 and AAM_2 were prepared for leaching during 7 d at 20 ± 1 °C. The percentages of Cs^+, Sr^{2+} and Na^+ leached under these new leaching conditions are given in **Table 6**.

Increasing the slag fineness of S_2 to a comparable value of that of S_5.1 (see **Table 4**) reduces the Cs^+ and Sr^{2+} release of AAM_2 by a factor 2, increasing its immobilisation capacity beyond that of AAM_5.1. AAM_1 shows the greatest immobilisation potential for all constituents at 20 °C, despite having the smallest Blaine specific surface area of the slag. Increasing the slag fineness of S_1 and S_2 demonstrates its significant effect on the immobilisation potential. The increased Blaine value of 220 m²/kg for S_1 (which is now comparable to that of S_1.1) further increases the immobilisation potential for all constituents. The same effect is observed for AAM_2. Increasing the slag fineness leads to a larger fraction of small slag particles that can be readily dissolved to form hydrate phases. This, in turn, raises the need for more charge-balancing ions, thus increasing the incorporation potential.

The results of the effect of leaching temperature, and the differences in specific surface area and slag fineness support the earlier established relationship between the immobilisation potential and design parameters Si/Al and Ca/(Si+Al). Leaching at 20 °C strengthens the conclusion that low Si/Al and Ca/(Si+Al) ratios provide a higher immobilisation potential since AAM_1 now exhibits the best immobilisation potential (see **Table 5** and **Table 6**). Under the experimental conditions, a Si/Al ratio of 1 thus seems optimal for immobilising Cs^+ and Sr^{2+}.

Table 6: Higher Blaine values (HB) after additional milling and $\%\ release$ after 7 d leaching at 20 °C of AAM_1 and AAM_2 prepared with HB-slag.

Sample	Slag Blaine HB (m²/kg)	$\%\ release$ 7 d, **20 °C**		
		Cs^+	Sr^{2+}	Na^+
AAM_1	220 ± 10	2.38	0.05	22.03
AAM_2	380 ± 10	12.79	0.18	31.48

4 Conclusion

The effect of AAM composition regarding Si/Al and Ca/(Si+Al) ratios on the immobilisation capacity of introduced Cs^+ and Sr^{2+} is discussed. Stoichiometrically controlled slags were designed from analytical grade chemicals to serve as precursors for monolithic AAM samples for immobilisation purposes. Under the given experimental conditions, the following conclusions are made:

a) Very effective immobilisation of Cs^+ and Sr^{2+} was achieved by use of low-alkaline AAMs. An immobilisation potential of up to 97.6 % and 99.9 % of introduced Cs^+ and Sr^{2+} respectively was achieved for composition AAM_1, after 7 days of leaching at 20 °C.
b) The leaching behaviour of Cs^+ from the AAMs consists of a combination of initial wash-off, diffusion and depletion of an easily-leachable fraction. Sr^{2+} leaching appears to be limited to a small fraction present on or near the surface, showing less wash-off and exhibiting slow depletion.
c) Cs^+ immobilisation is dependent on the Si/Al and Ca/(Si+Al) ratios of the precursor while Sr^{2+} immobilisation is only dependent on the Ca/(Si+Al) ratio. Better immobilisation is achieved at lower ratios, independent of the observed differences in precursor fineness or AAM specific surface area.
d) Lowering the leaching temperature from 90 °C to 20 °C has a varying effect on the immobilisation capacity of different compositions. This highlights the importance of being aware that leaching conditions affect obtained results, especially when comparing compositions. Leaching at higher temperature affects the curing of the AAMs, which can lead to misinterpretations of leaching results when comparing immobilisation capacities of different compositions.

In general, the developed AAMs show very effective Cs^+ and Sr^{2+} immobilisation which is very promising for the use of AAMs for waste immobilisation purposes. This study offers a deeper understanding of the immobilisation mechanism of AAMs, which could encourage further research in finding better alternatives for RAW immobilisation, and, in turn, encourage its large-scale application.

Acknowledgements

The authors thank Joris Van Dyck (KU Leuven, Department of Materials Engineering) for his assistance in developing the slag precursors, Elsy Thijssen and Martine Vanhamel (Hasselt University, CMK, Research Group of Applied and Analytical Chemistry) for their help regarding ICP-OES and ICP-MS measurements, and Bart Ruttens (IMEC, Division IMOMEC) for the XRD measurements.

Data availability

The raw/processed data required to reproduce these findings cannot be shared at this time as the data also forms part of an ongoing study.

References

[1] P. Krivenko, Why alkaline activation - 60 years of the theory and practice of alkali-activated materials, J. Ceram. Sci. Technol. 8 (2017) 323–333. doi:10.4416/JCST2017-00042.

[2] J.L. Provis, Introduction and scope, in: Alkali Act. Mater. State-of-the-Art Report, RILEM TC 224-AAM, 2014: pp. 1–9.

[3] W. Xuequan, Y. Sheng, S. Xiaodong, T. Mingshu, Y. Liji, Alkali-activated slag cement based radioactive waste forms, Cem. Concr. Res. 21 (1991) 16–20. doi:10.1016/0008-8846(91)90026-E.

[4] S. Xiaodong, Y. Sheng, W. Xuequan, T. Mingshu, Y. Liji, Immobilization of simulated high level wastes into AASC waste form, Cem. Concr. Res. 24 (1994) 133–138. doi:10.1016/0008-8846(94)90094-9.

[5] M.Y. Khalil, E. Merz, Immobilization of intermediate-level wastes in geopolymers, J. Nucl. Mater. 211 (1994) 141–148. doi:10.1016/0022-3115(94)90364-6.

[6] G. Qian, D.D. Sun, J.H. Tay, New aluminium-rich alkali slag matrix with clay minerals for immobilizing simulated radioactive Sr and Cs waste, J. Nucl. Mater. 299 (2001) 199–204. doi:10.1016/S0022-3115(01)00700-0.

[7] Q. Guangren, L. Yuxiang, Y. Facheng, S. Rongming, Improvement of metakaolin on radioactive Sr and Cs immobilization of alkali-activated slag matrix, J. Hazard. Mater. 92 (2002) 289–300.

doi:10.1016/S0304-3894(02)00022-5.

[8] A. Fernandez-Jimenez, D.E. MacPhee, E.E. Lachowski, A. Palomo, Immobilization of cesium in alkaline activated fly ash matrix, J. Nucl. Mater. 346 (2005) 185–193. doi:10.1016/j.jnucmat.2005.06.006.

[9] C. Shi, a. Fernández-Jiménez, Stabilization/solidification of hazardous and radioactive wastes with alkali-activated cements, J. Hazard. Mater. 137 (2006) 1656–1663. doi:10.1016/j.jhazmat.2006.05.008.

[10] S. Goni, A. Guerrero, M.P. Lorenzo, Efficiency of fly ash belite cement and zeolite matrices for immobilizing cesium, J. Hazard. Mater. 137 (2006) 1608–1617. doi:10.1016/j.jhazmat.2006.04.059.

[11] M.G. Blackford, J. V. Hanna, K.J. Pike, E.R. Vance, D.S. Perera, Transmission electron microscopy and nuclear magnetic resonance studies of geopolymers for radioactive waste immobilization, J. Am. Ceram. Soc. 90 (2007) 1193–1199. doi:10.1111/j.1551-2916.2007.01532.x.

[12] Z. Aly, E.R. Vance, D.S. Perera, J. V. Hanna, C.S. Griffith, J. Davis, D. Durce, Aqueous leachability of metakaolin-based geopolymers with molar ratios of Si/Al = 1.5-4, J. Nucl. Mater. 378 (2008) 172–179. doi:10.1016/j.jnucmat.2008.06.015.

[13] J.L. Provis, P.A. Walls, J.S.J. van Deventer, Geopolymerisation kinetics. 3. Effects of Cs and Sr salts, Chem. Eng. Sci. 63 (2008) 4480–4489. doi:10.1016/j.ces.2008.06.008.

[14] Q. Li, Z. Sun, D. Tao, Y. Xu, P. Li, H. Cui, J. Zhai, Immobilization of simulated radionuclide 133Cs+ by fly ash-based geopolymer, J. Hazard. Mater. 262 (2013) 325–331. doi:10.1016/j.jhazmat.2013.08.049.

[15] C. Kuenzel, J.F. Cisneros, T.P. Neville, L. Vandeperre, S.J.R. Simons, J. Bensted, C.R. Cheeseman, Encapsulation of Cs/Sr contaminated clinoptilolite geopolymers produced from metakaolin, J. Nucl. Mater. 466 (2015) 94–99.

[16] J.G. Jang, S.M. Park, H.K. Lee, Physical barrier effect of geopolymeric waste form on diffusivity of cesium and strontium, J. Hazard. Mater. 318 (2016) 339–346. doi:10.1016/j.jhazmat.2016.07.003.

[17] X. Peng, Y. Xu, Z. Xu, D. Wu, D. Li, Effect of simulated radionuclide strontium on geopolymerization process, Procedia Environ. Sci. 31 (2016) 325–329. doi:10.1016/j.proenv.2016.02.043.

[18] Z. Li, T. Ohnuki, K. Ikeda, Development of paper sludge ash-based geopolymer and application to treatment of hazardous water contaminated with radioisotopes, Materials (Basel). 9 (2016) 633. doi:10.3390/ma9080633.

[19] Z. Xu, Z. Jiang, D. Wu, X. Peng, Y. Xu, N. Li, Y. Qi, P. Li, Immobilization of strontium-loaded zeolite A by metakaolin based-geopolymer, Ceram. Int. 43 (2017) 4434–4439. doi:10.1016/j.ceramint.2016.12.092.

[20] J. Jang, S. Park, H. Lee, Cesium and strontium retentions governed by aluminosilicate gel in alkali-activated cements, Materials (Basel). 10 (2017). doi:10.3390/ma10040447.

[21] K. Shiota, T. Nakamura, M. Takaoka, S.F. Aminuddin, K. Oshita, T. Fujimori, Stabilization of cesium in alkali-activated municipal solid waste incineration fly ash and a pyrophyllite-based system, Chemosphere. 187 (2017) 188–195. doi:10.1016/j.chemosphere.2017.08.114.

[22] K. Shiota, T. Nakamura, M. Takaoka, K. Nitta, K. Oshita, T. Fujimori, T. Ina, Chemical kinetics of

Cs species in an alkali-activated municipal solid waste incineration fly ash and pyrophyllite-based system using Cs K-edge in situ X-ray absorption fine structure analysis, Spectrochim. Acta - Part B At. Spectrosc. 131 (2017) 32–39. doi:10.1016/j.sab.2017.03.003.

[23] J. Zhang, J.L. Provis, D. Feng, J.S.J. van Deventer, Geopolymers for immobilization of Cr6+, Cd2+, and Pb2+, J. Hazard. Mater. 157 (2008) 587–598. doi:10.1016/j.jhazmat.2008.01.053.

[24] T. Hanzlicek, M. Steinerova, P. Straka, Radioactive metal isotopes stabilized in a geopolymer matrix: Determination of a leaching extract by a radiotracer method, J. Am. Ceram. Soc. 89 (2006) 3541–3543. doi:10.1111/j.1551-2916.2006.01024.x.

[25] P. Lichvar, M. Rozloznik, S. Sekely, Behaviour of aluminosilicate inorganic matrix SIAL® during and after solidification of radioactive sludge and radioactive spent resins and their mixtures, Proc. IAEA Meet. Kalpakkam, India. (2010).

[26] M.R. El-Naggar, Applicability of alkali activated slag-seeded Egyptian Sinai kaolin for the immobilization of 60Co radionuclide, J. Nucl. Mater. 447 (2014) 15–21. doi:10.1016/j.jnucmat.2013.12.020.

[27] International Atomic Energy Agency, The behaviours of cementitious materials in long term storage and disposal of radioactive waste : results of a coordinated research project, Vienna, 2013.

[28] European Committee for Standardization, EN 196-6:2010 - Methods of testing cement - Part 6: Determination of fineness, 2010.

[29] N. Vandevenne, R.I. Iacobescu, Y. Pontikes, R. Carleer, E. Thijssen, K. Gijbels, S. Schreurs, W. Schroeyers, Incorporating Cs and Sr into blast furnace slag inorganic polymers and their effect on matrix properties, J. Nucl. Mater. 503 (2018) 1–12. doi:10.1016/j.jnucmat.2018.02.023.

[30] N. Vandevenne, R.I. Iacobescu, Y. Pontikes, K. Gijbels, S. Schreurs, W. Schroeyers, The effect of Cs and Sr on the mechanical properties of blast furnace slag inorganic polymer for radioactive waste immobilisation, in: 5th Int. Slag Valoris. Symp., 2017: pp. 401–404.

[31] ASTM, C 1220 - 98 Standard test method for static leaching of monolithic waste forms for disposal of radioactive waste, (1998).

[32] European Committee for Standardization, CEN/TS 15863:2015: Characterisation of waste - Leaching behaviour test for basic characterisation - Dynamic monolithic leaching test with periodic leachant renewal, under fixed test conditions, 2015.

[33] H.A. van der Sloot, J.J. Dijkstra, Development of horizontally standardized leaching tests for construction materials: a material based or release based approach?, (2004) 56.

[34] A.C. Garrabrants, D.S. Kosson, H.A. Van Der Sloot, F. Sanchez, O. Hjelmar., Background information for the Leaching Environmental Assessment Framework (LEAF) test methods, U.S. Environ. Prot. Agency, Washington, DC,. (2011).

[35] D.S. Kosson, H.A. van der Sloot, F. Sanchez, A.C. Garrabrants, An integrated framework for evaluating leaching in waste management and utilization of secondary materials, Environ. Eng. Sci. 19 (2002) 159–204. doi:10.1089/109287502760079188.

[36] R.J. Myers, S.A. Bernal, J.L. Provis, A thermodynamic model for C-(N-)A-S-H gel: CNASH-ss. Derivation and validation, Cem. Concr. Res. 66 (2014) 27–47. doi:10.1016/j.cemconres.2014.07.005.

[37] R.J. Myers, B. Lothenbach, S.A. Bernal, J.L. Provis, Thermodynamic modelling of alkali-activated slag cements, Appl. Geochemistry. 61 (2015) 233–247.

doi:10.1016/j.apgeochem.2015.06.006.

[38] B. Walkley, R. San Nicolas, M.A. Sani, G.J. Rees, J. V. Hanna, J.S.J. van Deventer, J.L. Provis, Phase evolution of C-(N)-A-S-H/N-A-S-H gel blends investigated via alkali-activation of synthetic calcium aluminosilicate precursors, Cem. Concr. Res. 89 (2016) 120–135. doi:10.1016/j.cemconres.2016.08.010.